II International Conference on Particle-based Methods - Fundamentals and Applications
PARTICLES 2011
E. Oñate and D.R.J. Owen (Eds)

# SIMULATING FLUID-SOLID INTERACTION PROBLEMS USING AN IMMERSED BOUNDARY-SPH METHOD

**Mohammad Reza Hashemi*, Rouhollah Fatehi† and Mehrdad T. Manzari***

*Center of Excellence in Energy Convergence
School of Mechanical Engineering
Sharif University of Technology, Tehran, Iran

†Department of Mechanical Engineering
School of Engineering
Persian Gulf University, Bushehr, Iran

**Key words:** SPH, IBM, Particulate Flow, Fluid-Solid Interaction

**Abstract.** In this work, the Immersed Boundary Method (IBM) is adapted and implemented in the context of Smoothed Particle Hydrodynamics (SPH) method to study moving solid bodies in an incompressible fluid flow. The proposed computational algorithm is verified by solving a number of benchmark particulate flow problems. The results are also compared with those obtained using the same SPH scheme along with a direct solid boundary imposition technique.

## 1 Introduction

The rheological characteristics of particulate flows are of prime interest in many industries. These macroscopic characteristics can be described by various hydrodynamic interactions between solids and the surrounding fluid. To investigate such interactions, one needs to accurately determine the hydrodynamic forces exchanged between the fluid and solid bodies.

This paper attempts to numerically simulate particulate flows using a combination of the Weakly Compressible SPH (WCSPH) and the Immersed Boundary (IB) method. The use of immersed boundary method helps to handle problems with solid bodies of complex geometries as reported by Hieber and Koumoutsakos [1]. They used a combination of the IB and the SPH method, however, brought the SPH particles back into an ordered arrangement at the end of each time step. In the present paper, the IB method is used along with a modified scheme of the WCSPH method.

It is known that in the IB method, the portion of the fluid domain confined within solid boundaries, imposes a retarding effect on the motion of solid bodies [2]. This effect leads to an under estimation of the acceleration of the solid bodies. In 2005, Uhlmann [2] proposed

that the momentum of this confined fluid should be taken into account in order to resolve the problem. In this work, this effect is relieved using a momentum rate summation over SPH particles positioned inside a solid body.

In this paper, some modifications are also used in order to improve capabilities of the standard WCSPH method. The so-called Renormalized schemes are used for the first-order and second-order spatial derivatives. Also, the spurious pressure oscillations are reduced using a modified continuity equation.

In the following, first the proposed weakly compressible SPH method is described. This is followed by presenting the direct fluid-solid boundary treatment and the equation of motion of the solid bodies. Next, the IB method and the time integration procedure are briefly described. Finally, the performance of the proposed method is studied by solving migration of a circular cylinder in a shear flow and falling of a circular solid body in a closed channel. Comparisons between the results of the proposed IB-SPH method and those obtained using the same SPH scheme with a direct solid boundary imposition technique, are also performed.

## 2 The SPH Method

In this work, weakly-compressible laminar fluid flows are considered. The mass and momentum conservation laws give

$$\frac{d\rho}{dt} = -\rho \nabla \cdot \mathbf{V}, \tag{1}$$

$$\rho \frac{d\mathbf{V}}{dt} = -\nabla P + \mu \nabla^2 \mathbf{V}, \tag{2}$$

where $\rho$ is density of the fluid, $P$ is pressure and $\mathbf{V}$ is the velocity vector. In order to close this system of equations, a simple equation of state is used as

$$P - P_0 = c^2(\rho - \rho_0). \tag{3}$$

Equations (1) and (2) are solved using the SPH method as discussed below.

### 2.1 Spatial Derivatives

The numerical approximation of the first derivative, $\langle \nabla u \rangle_i$, can be obtained as [3, 4]

$$\langle \nabla u \rangle_i = \mathbf{B}_i \cdot \sum_j \omega_j \nabla W_{ij} \left( u_j - u_i \right), \tag{4}$$

where $W_{ij} = W(|\mathbf{r}_{ij}|, h)$ refers to the value of smoothing or kernel function of particle $i$ at the position of particle $j$ and $\mathbf{r}_{ij} = \mathbf{r}_i - \mathbf{r}_j$. Also,

$$\mathbf{B}_i = -\left[ \sum_j \omega_j \mathbf{r}_{ij} \nabla W_{ij} \right]^{-1} \tag{5}$$

is a renormalization tensor. Using Taylor series expansion about $\mathbf{r}_i$, it can be shown that the method described by Eq. (4) is consistent and converges linearly as $\delta \longrightarrow 0$ for a constant ratio $\frac{h}{\delta}$ [4].

A consistent second derivative approximation scheme was recently introduced by Fatehi and Manzari [4] as

$$\left\langle \nabla^2 u \right\rangle_i = \hat{\mathbf{B}}_i : \sum_j 2\omega_j \mathbf{e}_{ij} \nabla W_{ij} \left( \frac{u_i - u_j}{r_{ij}} - \mathbf{e}_{ij} \cdot \left\langle \nabla u \right\rangle_i \right), \tag{6}$$

where the operator ":" denotes the inner product of second-order tensors, $r_{ij} = |\mathbf{r}_{ij}|$, $\mathbf{e}_{ij} = \mathbf{r}_{ij}/r_{ij}$ is a unit vector in the inter-particle direction and $\left\langle \nabla u \right\rangle_i$ is computed according to (4). $\hat{\mathbf{B}}$ is a renormalization tensor which is computed using the following set of equations

$$\hat{\mathbf{B}}_i : \left[ \sum_j \omega_j \mathbf{r}_{ij} \mathbf{e}_{ij} \mathbf{e}_{ij} \nabla W_{ij} + \left( \sum_j \omega_j \mathbf{e}_{ij} \mathbf{e}_{ij} \nabla W_{ij} \right) \cdot \mathbf{B}_i \cdot \left( \sum_j \omega_j \mathbf{r}_{ij} \mathbf{r}_{ij} \nabla W_{ij} \right) \right] = -\mathbf{I}. \tag{7}$$

These schemes are directly applied to the momentum equation (2). The discretization of the mass conservation equation (1) is described below.

### 2.2 Modified Mass Conservation Equation

Lee *et al.* [5] reported that a Weakly Compressible SPH formulation may lead to spurious pressure oscillations. As discussed in [6], a modification to the continuity equation can solve this problem. Here, the mass conservation equation (1) is replaced by [7]

$$\frac{d\rho_i}{dt} = -\rho_i \left[ \left\langle \nabla \cdot \mathbf{V} \right\rangle_i + \Delta t \left( \left\langle \nabla \cdot \left\langle \frac{\nabla P}{\rho} \right\rangle \right\rangle_i - \left\langle \nabla \cdot \frac{\nabla P}{\rho} \right\rangle_i \right) \right], \tag{8}$$

in which

$$\left\langle \nabla \cdot \left\langle \frac{\nabla P}{\rho} \right\rangle \right\rangle_i = \mathbf{B}_i \cdot \sum_j \omega_j \nabla W_{ij} \cdot \left( \left\langle \frac{\nabla P}{\rho} \right\rangle_j - \left\langle \frac{\nabla P}{\rho} \right\rangle_i \right), \tag{9}$$

and

$$\left\langle \nabla \cdot \frac{\nabla P}{\rho} \right\rangle_i = \hat{\mathbf{B}}_i : \sum_j 2\omega_j \mathbf{e}_{ij} \nabla W_{ij} \left( \frac{P_i - P_j}{\bar{\rho}_{ij} r_{ij}} - \mathbf{e}_{ij} \cdot \left\langle \frac{\nabla P}{\rho} \right\rangle_i \right), \tag{10}$$

where $\bar{\rho}_{ij} = (\rho_i + \rho_j)/2$.

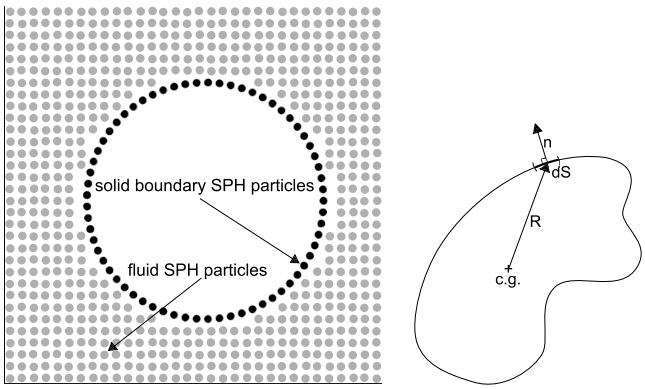


Figure 1: a) Initial SPH particles arrangement near a solid body for direct boundary treatment method, and b) schematic of solid body diagram.

### 2.3 Direct Solid Boundary Treatment

Proper evaluation of the hydrodynamic forces is an essential part of simulating particulate flow problems. In the direct treatment of the solid boundaries, the solid boundaries are represented by one layer of SPH particles, as shown in Fig. 1-a, which leads to a fairly smooth and accurate pressure distribution around the solid bodies. To find the pressure and density of a boundary particle, the fluid equation of motion needs to be solved. Adjacent to a solid surface, the momentum conservation equation can be rewritten as

$$\frac{\nabla P}{\rho} \cdot \mathbf{n} = -\frac{d\mathbf{V}}{dt} \cdot \mathbf{n} + \frac{\nabla \cdot \tau}{\rho} \cdot \mathbf{n}, \tag{11}$$

where $\mathbf{n}$ is the unit outward normal to the solid surface. For the boundary particle $i$, $\mathbf{n}_i$ can be calculated from the summation of the kernel gradients [3] as

$$\mathbf{n}_i = \frac{\sum_j \omega_j \nabla W_{ij}}{\left| \sum_j \omega_j \nabla W_{ij} \right|}. \tag{12}$$

Discretizing the pressure gradient term in (11) for particle $i$, leads to

$$\left( \sum_j \omega_j \frac{P_j - P_i}{\bar{\rho}_{ij}} \mathbf{B}_i \cdot \nabla W_{ij} \right) \cdot \mathbf{n}_i = -\frac{d\mathbf{V}_i}{dt} \cdot \mathbf{n}_i + \left\langle \frac{\nabla \cdot \tau}{\rho} \right\rangle_i \cdot \mathbf{n}_i. \tag{13}$$

The term $\frac{d\mathbf{V}_i}{dt}$ is the acceleration of the boundary particle $i$ which is evaluated in terms of the predicted acceleration of the corresponding solid body at each time step. Therefore, $P_i$ can be found explicitly from (13), and $\rho_i$ is easily updated using the fluid equation of state.

## 3 Solid Body Equation of Motion

The Newton's law of motion is used to explicitly update the solid body velocity and position. For a solid body $b$, the linear and angular momentum equations are

$$M_b \frac{d\mathbf{V}_b}{dt} = \mathbf{f}_b, \tag{14}$$

and

$$I_b \frac{d\mathbf{\Omega}_b}{dt} = \mathbf{m}_b, \tag{15}$$

where $M_b$ and $I_b$ are the total mass and moment of inertia of the body, respectively, and, $\mathbf{\Omega}_b$ is the angular velocity vector. In (14) and (15), $\mathbf{f}_b$ and $\mathbf{m}_b$ are the hydrodynamic force and moment exerted on the surface of the solid body and are approximated by summations over the boundary particles, as

$$\mathbf{f}_b = \sum_j \left(-P_j \mathbf{n}_j + \mathbf{n}_j \cdot \tau_j\right) \Delta S_j \tag{16}$$

and

$$\mathbf{m}_b = \sum_j \mathbf{R}_j \times \left(-P_j \mathbf{n}_j + \mathbf{n}_j \cdot \tau_j\right) \Delta S_j, \tag{17}$$

where $\Delta S_j$ denotes a portion of the solid surface. $\mathbf{R}_j$ is the position vector from the center of solid body $b$ as shown in Fig. 1-b. These parameters are associated with the boundary particle $j$.

## 4 The Immersed Boundary Method

The Immersed Boundary (IB) method was introduced in 1977 [8] in order to impose a complicated no-slip boundary condition. This method can also eliminate the limitations associated with the moving solid boundaries in particle methods [1]. In order to implement the IB method in the context of SPH, considering the idea introduced in [2], the force and moment in the solid body equations of motion (14) and (15) become

$$\mathbf{f}_b = \sum_k \mathbf{F}_k + \sum_i m_i \frac{d\mathbf{V}_i}{dt} \tag{18}$$

$$\mathbf{m}_b = \sum_k \mathbf{R}_k \times \mathbf{F}_k + \sum_i m_i \mathbf{R}_k \times \frac{d\mathbf{V}_i}{dt}, \tag{19}$$

where the subscript $k$ refers to boundary points, $i$ stands for the confined SPH particles within the solid body $b$. The second terms in the RHS of Eqs. (18) and (19) resolve the miscalculation of the solid body acceleration. Figure 2 shows a schematic of the interaction forces between the boundary points and the fluid SPH particle.

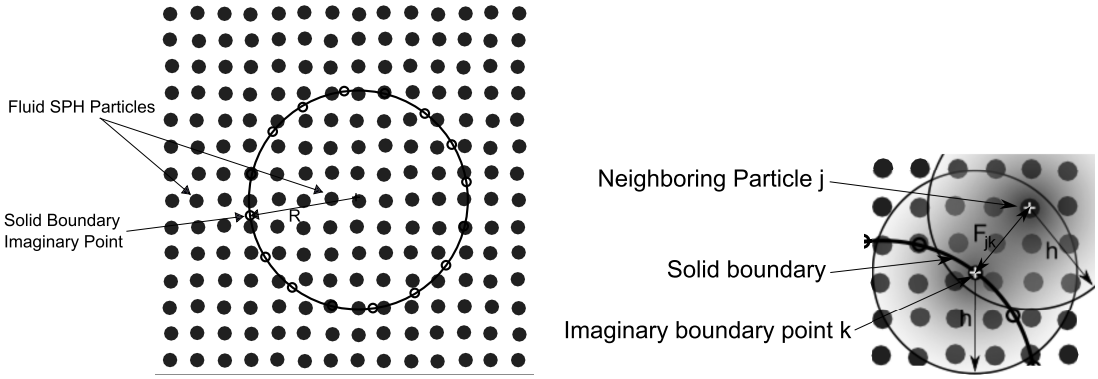


Figure 2: Schematic view of the boundary points and interaction forces between the points and fluid SPH particles.

The interaction forces $F_k$ which act on each boundary point are calculated using the difference between a predicted velocity due to the rigid motion of the solid bodies and the interpolated fluid velocity at the position of the point $k$. The velocity interpolation is done using a kernel function and a summation over the fluid SPH particles $j$ in the neighborhood of the boundary point $k$, as

$$\mathbf{V}_k^* = \sum_j c_{kj} \mathbf{V}_j^*. \tag{20}$$

$\mathbf{V}^*$ is evaluated assuming that there is no solid body in the domain and $c_{kj} = \omega_j W_{kj} / \sum_j \omega_j W_{kj}$. Denoting the predicted velocity of the boundary point $k$ by $\mathbf{V}_k^d$, one has

$$\mathbf{f}_k = \frac{\mathbf{V}_k^* - \mathbf{V}_k^d}{\Delta t}, \tag{21}$$

where $\Delta t$ is the time step size. The force acting on the fluid SPH particle $j$ due to the presence of its neighboring boundary points $k$ is

$$\mathbf{F}_j = \sum_k c_{kj} \mathbf{F}_{kj}, \tag{22}$$

with

$$\mathbf{F}_{kj} = -m_j c_{jk} \mathbf{f}_k. \tag{23}$$

Thus, the velocity of the SPH particle $j$ should be updated as

$$\mathbf{V}_j = \mathbf{V}_j^* + \Delta t \frac{\mathbf{F}_j}{m_j}. \tag{24}$$

Finally, $\mathbf{F}_k$ is calculated as

$$\mathbf{F}_k = -\sum_j c_{jk} \mathbf{F}_{kj}. \tag{25}$$

It must be noted that the only difference in using the IB technique in combination with the proposed SPH method is that equations (16) and (17), which are calculated using the direct solid boundary treatment method, are replaced by Eqs. (18) and (19).

## 5 Time Integration

To solve the governing equations in time, a two-step predictor-corrector method is used. First, velocity $\mathbf{V}^*$ and density $\rho^*$ are predicted solving the equations of motions. Then, the pressure field is updated using $\rho^*$ in (3). Next, the corrected values $\mathbf{V}^{**}$ and $\rho^{**}$ are calculated, solving flow equations using the predicted ($^*$) values. The new values of velocity, density, and position are then computed sequentially using

$$\mathbf{V}^{n+1} = \frac{1}{2}\left(\mathbf{V}^{**} + \mathbf{V}^{*}\right), \tag{26}$$

$$\rho^{n+1} = \frac{1}{2}\left(\rho^{**} + \rho^{*}\right), \tag{27}$$

and

$$\mathbf{r}^{n+1} = \mathbf{r}^{n} + \Delta t \mathbf{V}^{n+1}. \tag{28}$$

Here, $\Delta t = t^{n+1} - t^n$ and after stability analysis one finds that $\Delta t$ must be constrained by [9]

$$\Delta t = \alpha \min\left(\frac{\delta_{min}}{U_{max}}, \frac{\rho \delta_{min}^2}{\mu}\right). \tag{29}$$

Here, $0 < \alpha < 1$ is a constant, $\delta_{min}$ is the minimum distance between two neighboring SPH particles, $U_{max} = c + V_{max}$ is the maximum characteristic velocity, $c$ is the speed of sound which appears in (3) and $V_{max}$ is the maximum velocity of the SPH particles. It must be noted that, both linear and angular velocities of the moving solid bodies are also updated, using (14) and (15) in every predictor and corrector steps and finally averaged in the same way as the fluid SPH particles.

During a SPH simulation, defects may be produced by non-uniform distribution and clustering of SPH particles. To alleviate this problem, Xu and his co-workers proposed a particle shifting defined by $\delta\mathbf{r}_i$ [10] as

$$\delta\mathbf{r}_i = \beta V_{max} \Delta t \sum_j \frac{\overline{r}_i^2}{r_{ij}^2} \mathbf{e}_{ij}, \tag{30}$$

where $\overline{r}_i = \frac{1}{N_i}\sum_j r_{ij}$, and $N_i$ is the number of neighboring particles for particle $i$. The constant $\beta$, should be within the range $0.001 - 0.1$ to prevent numerical instability and large errors [10]. In this work, the same modification is used in the context of Weakly Compressible SPH (WCSPH) method.

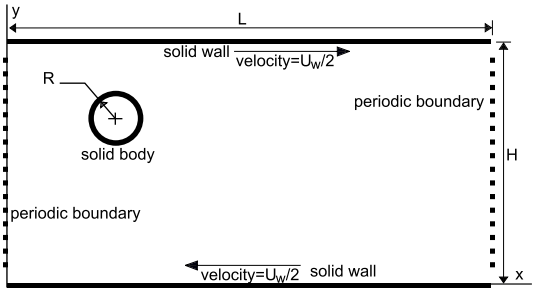


**Figure 3**: Schematic diagram of the circular cylinder in a shear flow.

## 6 Results

In this section, the proposed method is verified by solving two planar low-Reynolds benchmark problems. First, the migration of a neutrally buoyant solid body in a shear flow is simulated, and secondly, the problem of a falling solid body under the effect of gravity force, in a closed channel is solved. For all simulations, a Quintic Wendland kernel function [11] is used with a cut-off distance $h$ of 2.6 times the initial SPH particle spacing, $\delta_0$. The sound speed $c$ in (3) is chosen to be almost 20 times the maximum velocity in the domain to ensure the incompressibility condition [12] and the constant $\alpha$ in (29) is set to 0.5.

### 6.1 A Neutrally Buoyant Circular Cylinder in a Shear Flow

In this problem, a neutrally buoyant rigid circular cylinder is free to move in a shear flow as shown in Fig. 3. The height of the channel, $H$, is $0.01(m)$ and the ratio of solid body radius to the channel height is $R/H = 1/8$. The velocities of the upper and the lower walls are equal to $U_w/2 = 0.01(m/s)$ in opposite directions. The particle Reynolds number, $Re_p = U_w R^2/(\nu H)$, for which the results were reported in [13], is 0.625. The solid body is initially at rest positioned at $y = 0.75H$. The left and right sides of the channel are periodic boundaries.

Here, the length to height ratio of the channel, $L/H$, is set to 5, which ensures that results are independent from the chosen channel length. Also, $\beta = 0.01$ and $c = 0.25(m/s)$. In Fig. 4, the vertical positions of the solid body is shown in time, for both the direct solid boundary treatment and the IB method. The results are compared with those reported by Z-G Feng [13] in 2002. In this problem, the initial SPH particle spacing is $\delta_0 = 1/6000(m)$. It is observed that the result obtained using the WCSPH method is almost the same as those shown in [13]. However, for the IB method some oscillations occur when the solid body reaches the centerline of the channel.

### 6.2 Falling of a Circular Cylinder in a Closed Channel

In this problem, a circular cylinder starts to move from rest under the gravity effect, with $g = 9.81(m/s^2)$. A schematic geometry of the problem is shown in Fig. 5. The

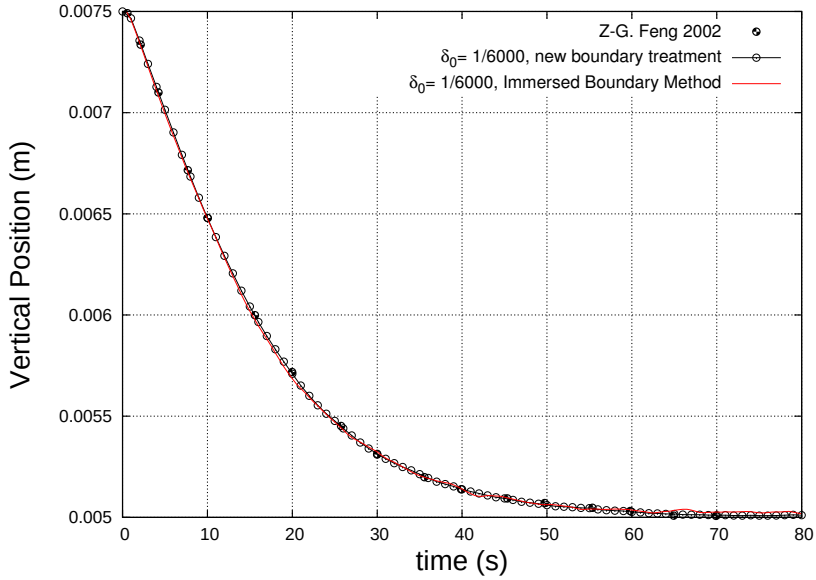


**Figure 4**: Vertical position of the solid body in comparison with [13].

domain dimensions are $H = 0.06(m)$ and $L = 0.02(m)$, the radius of solid cylinder $R = 0.00125(m)$ and the center of the solid is initially at $x = 0.01(m)$ and $y = 0.04(m)$. The solid and fluid densities are, respectively, $\rho_s = 1250(kg/m^3)$ and $\rho_f = 1000(kg/m^3)$, and the fluid viscosity is $\mu = 0.01(Pa.s)$.

Here, $\beta = 0.02$ and $c = 1.0(m/s)$. In Fig. 6 the calculated vertical velocities of the falling solid body, for both the direct solid boundary treatment and the IB method, are compared with the result reported in [14]. In this problem, the initial SPH particle spacing is $\delta_0 = 1/10000(m)$. Although the results are in good agreement, some oscillations appear in the velocity when the solid body reaches its terminal velocity. These occur as a result of small pressure oscillations imposed by the pressure waves produced in a weakly compressible fluid. In this problem, the acceleration of the solid body changes from the gravity acceleration at the beginning to zero when a terminal velocity is achieved. Thus the performance of the solid boundary treatment methods can be assessed. While the solid body is falling with a variable velocity, the direct boundary treatment method performs better. On the other hand, when the solid body reaches its terminal falling velocity, the results obtained using the IB method are in a better agreement with those reported in [14].

## 7 Conclusion

Both direct solid boundary treatment and the IB method performed well in particulate flow simulations. However, the results obtained using the direct boundary treatment method were in a better agreement with the results available in the literature while the solid body was moving with a variable velocity. On the other hand the IB method gave

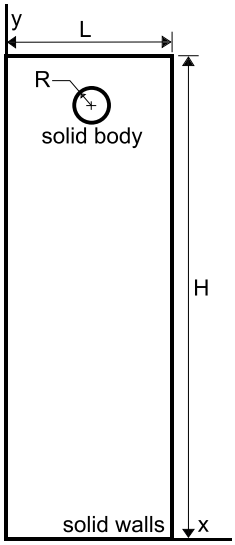


**Figure 5**: Schematic diagram of the falling circular cylinder in a closed channel.

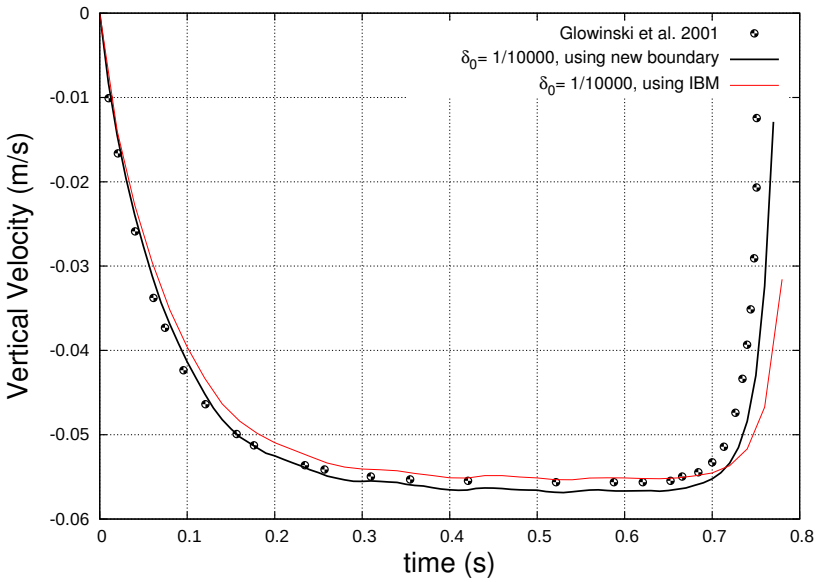


**Figure 6**: Vertical velocity of the falling particle in a closed channel in comparison with [14].

a more accurate result at the terminal velocity.

## REFERENCES

[1] S. Hieber and P. Koumoutsakos, "An immersed boundary method for smoothed particle hydrodynamics of self-propelled swimmers," *Journal of Computational Physics*, vol. 227, no. 19, pp. 8636–8654, 2008.

[2] M. Uhlmann, "An immersed boundary method with direct forcing for the simulation of particulate flows," *Journal of Computational Physics*, vol. 209, no. 2, pp. 448–476, 2005.

[3] P. W. Randles and L. D. Libersky, "Smoothed Particle Hydrodynamics: some recent improvements and applications," *Computer Methods in Applied Mechanics and Engineering*, vol. 139, no. 1-4, pp. 375–408, 1996.

[4] R. Fatehi and M. T. Manzari, "Error estimation in smoothed particle hydrodynamics and a new scheme for second derivatives," *Computers & Mathematics with Applications*, vol. 61, no. 2, pp. 482 – 498, 2011.

[5] E. S. Lee, C. Moulinec, R. Xu, D. Violeau, D. Laurence, and P. Stansby, "Comparisons of weakly compressible and truly incompressible algorithms for the SPH mesh free particle method," *Journal of Computational Physics*, vol. 227, no. 10, pp. 8417–8436, 2008.

[6] R. Fatehi and M. T. Manzari, "A remedy for numerical oscillations in weakly compressible smoothed particle hydrodynamics," *International Journal for Numerical Methods in Fluids*, 2010. In press. [Available online: http://dx.doi.org/10.1002/fld.2406]

[7] R. Fatehi and M. T. Manzari, "A consistent and fast weakly compressible sph with a new wall boundary condition," *International Journal for Numerical Methods in Fluids*, 2011. In press. [Available online: http://dx.doi.org/10.1002/fld.2586]

[8] C. Peskin, "Numerical analysis of blood flow in the heart," *Journal of Computational Physics*, vol. 25, no. 3, pp. 220–252, 1977.

[9] S. Shao and E. Y. M. Lo, "Incompressible SPH method for simulating newtonian and non-newtonian flows with a free surface," *Advances in Water Resources*, vol. 26, no. 7, pp. 787–800, 2003.

[10] R. Xu, P. Stansby, and D. Laurence, "Accuracy and stability in incompressible SPH (ISPH) based on the projection method and a new approach," *Journal of Computational Physics*, vol. 228, no. 18, pp. 6703 – 6725, 2009.

[11] H. Wendland, "Piecewise polynomial, positive definite and compactly supported radial functions of minimal degree," *Advances in Computational Mathematics*, vol. 4, no. 1, pp. 389–396, 1995.

[12] J. P. Morris, P. J. Fox, and Y. Zhu, "Modeling low Reynolds number incompressible flows using SPH," *Journal of Computational Physics*, vol. 136, no. 1, pp. 214–226, 1997.

[13] Z. Feng and E. Michaelides, "Interparticle forces and lift on a particle attached to a solid boundary in suspension flow," *Physics of fluids*, vol. 14, p. 49, 2002.

[14] R. Glowinski, T. Pan, T. Hesla, D. Joseph, and J. Periaux, "A distributed Lagrange multiplier/fictitious domain method for the simulation of flow around moving rigid bodies: application to particulate flow," *Computer methods in applied mechanics and engineering*, vol. 184, no. 2-4, pp. 241–267, 2000.